

3D-printed peristaltic microfluidic systems fabricated from thermoplastic elastomer

Jingyi Wang^{1,2} · Carlton McMullen³ · Ping Yao^{1,2} · Niandong Jiao¹ · Min Kim^{4,5} · Jin-Woo Kim⁵ · Lianqing Liu¹ · Steve Tung^{1,3}

Received: 24 January 2017 / Accepted: 15 May 2017 / Published online: 2 June 2017
© Springer-Verlag Berlin Heidelberg 2017

Abstract Recent advancements in 3D printing technology have provided a potential low-cost and time-saving alternative to conventional PDMS (polydimethylsiloxane)-based microfabrication for microfluidic systems. In addition to reducing the complexity of the fabrication procedure by eliminating such intermediate steps as molding and bonding, 3D printing also offers more flexibility in terms of structural design than the PDMS micromolding process. At present, 3D-printed microfluidic systems typically utilize a relatively ‘stiff’ printing material such as ABS (acrylonitrile butadiene styrene copolymers), which limits the implementation of large mechanical actuation for active pumping and mixing as routinely carried out in a PDMS system. In this paper, we report the development of an active 3D-printed microfluidic system with moving parts fabricated from a flexible thermoplastic elastomer (TPE). The 3D-printed microfluidic system consists of two pneumatically actuated

micropumps and one micromixer. The completed system was successfully applied to the detection of low-level insulin concentration using a chemiluminescence immunoassay, and the test result compares favorably with a similarly designed PDMS microfluidic system. Prior to system fabrication and testing, the material properties of TPE were extensively evaluated. The result indicated that TPE is compatible with biological materials and its 3D-printed surface is hydrophilic as opposed to hydrophobic for a molded PDMS surface. The Young’s modulus of TPE is measured to be 16 MPa, which is approximately eight times higher than that of PDMS, but over one hundred times lower than that of ABS.

Keywords Microfluidic system · 3D printing · Insulin detection

1 Introduction

The fabrication material for microfluidic systems has gone through several iterations, starting from the original silicon-based semiconducting materials (Ratner et al. 2005), to glass (Stjernstrom and Roeraade 1998), and to the latest organic polymers such as PMMA (polymethylmethacrylate) and PDMS, with PDMS being the most popular and widely used in recent years. As a microfabrication material, PDMS has a number of well-established advantages over silicon and glass including low cost, robustness, and biocompatibility (Thangawng et al. 2007). For microfluidic systems with moving parts, PDMS is especially valuable due to its relatively low elastic modulus, which allows flexible structures such as thin diaphragms to be fabricated and actuated with relative ease (Lai and Folch 2011). PDMS microfluidic

✉ Lianqing Liu
lqliu@sia.cn

✉ Steve Tung
chstung@uark.edu

¹ State Key Lab of Robotics, Shenyang Institute of Automation, Chinese Academy of Sciences, Shenyang, China
² University of Chinese Academy of Sciences, Beijing, China
³ Department of Mechanical Engineering, University of Arkansas, Fayetteville, AR, USA
⁴ Department of Physics, Williams College, Williamstown, MA, USA
⁵ Bio/Nano Technology Laboratory, Department of Biological and Agricultural Engineering, Institute for Nanoscience and Engineering, University of Arkansas, Fayetteville, AR, USA

systems have found applications in a wide range of chemical and biochemical assays where repeatability, short response time, and increased automation and system integration are important (Yao et al. 2016). To fulfill these needs, PDMS microfluidic systems typically incorporate active fluid pumping, valving, sorting, and mixing onto a single integrated platform where the assay parameters can be accurately controlled (Yao et al. 2013b).

The microfabrication process for PDMS microfluidic systems is very well established. Fundamentally, it is a micromolding and bonding technique where thin PDMS layers are first molded into planar structures using pre-designed micromasters fabricated from photoresist or PMMA. The molded PDMS layers are then thermally cured and align-bonded to complete the fabrication process. Frequently, a glass substrate is added to the bonded PDMS layers to increase structural rigidity for device handling and fluid input/output purposes (Plecis and Chen 2007). The PDMS microfabrication process is very labor intensive. The micromolding and bonding steps require trained personnel, and the curing process can take up to several hours to complete. Whenever changes in the PDMS structures are needed, new micromasters must be re-designed and fabricated, adding to the turnaround time of the new system. In terms of structural design, since micromolded PDMS layers consist mostly of planar structures, it is frequently difficult to incorporate novel three-dimensional elements often into the design of a PDMS microfluidic system.

This paper describes a new polymer microfluidic system designed and fabricated directly from the design software of a low-cost extrusion (fused deposition modeling or FDM)-based 3D printer. It is an active microfluidic system with pneumatically controlled pumping and mixing that is monolithically integrated into a common platform. 3D printing is a rapid prototyping technique that allows complex structures to be manufactured directly from design software without the need for intermediate processing steps. Lately, the cost for desktop extrusion-based 3D printing has declined significantly and the printing resolution of 20–100 μm has approached that of PDMS microfabrication. The 3D-printed microfluidic system described in this paper employs a TPE as the fabrication material, allowing flexible diaphragms to be incorporated into the microfluidic system as mechanical actuators to pump and mix sample fluids, similar to the pneumatic PDMS devices reported in our previous work (Yao et al. 2013a). 3D-printed microfluidic devices have been previously reported using stereolithography (SL) (Au et al. 2015; Sochol et al. 2016), polypropylene (Kitson et al. 2012), and ABS (Lee et al. 2016). The photopolymer used in SL, polypropylene, and ABS is typically stiff, making it difficult to design compliant diaphragms for pneumatic actuation. The Young's modulus of TPE is much lower than that of these materials.

In this paper, we describe the mechanical properties of TPE, demonstrate its biocompatibility behavior, design and 3D print an integrated TPE microfluidic system, characterize the pumping and mixing capabilities, and apply the 3D-printed microfluidic system to biomedical detection. In addition, the hydrophobicity and water absorption characteristics of TPE, two important material properties for microfluidic applications, are examined. The flow rate of the 3D-printed micropump and the mixing efficiency of the micromixer are tested under different pneumatic pressures and actuation frequencies. Finally, the completed microfluidic system is used to detect insulin concentration through a chemiluminescence immunoassay and the test result is compared with that obtained from a similarly designed PDMS microfluidic system.

2 Materials and methods

2.1 Extrusion-based 3D printing

Figure 1 demonstrates the schematics of extrusion-based 3D printing. The nozzle of the 3D printer melts the TPE filament and deposits it in a crisscross pattern on a build plate where the material cools and solidifies into a cohesive layer on the x - y plane. Once the first layer is completed, the nozzle traverses above the layer and repeats the process.

TPE is a biphasic material with the combined properties of a semicrystalline thermoplastic and a soft elastomer (Holden 2000). The rigid domains in TPE form a three-dimensional network of physical cross-link sites owing to the covalent linkages between chemically dissimilar segments (Shankar et al. 2010). Additionally, TPE exhibits mechanical properties similar to vulcanized rubber (Spontak and Patel 2000). The thermal reversibility nature of TPE makes it ideally suitable for melt extrusion and injection molding (Legge et al. 1987). Currently, commercially available TPEs suitable for 3D printing include NinjaFlex (Fenner Drives Inc.), Filaflex (Recreus), and MakerBot Flexible Filament (MakerBot

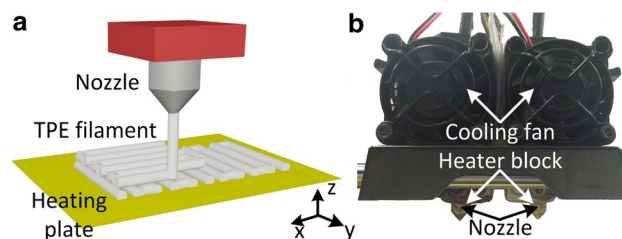


Fig. 1 **a** Schematic diagram of extrusion-based 3D printing. **b** Photograph showing the twin nozzles, heater block, and cooling fans of a 3D printer (Wanhao duplicator 4X). In the present work, only one nozzle is used to print TPE

Industries, LLC). We chose NinjaFlex for our microfluidic system fabrication because it is readily available and known to be reasonably flexible. In addition, based on our preliminary testing, NinjaFlex also has a relatively low water uptake properties, which keeps the material from swelling when exposed to water. However, NinjaFlex is not a standard extrusion-based printing material such as ABS and PLA (polylactide). Its flexibility can cause frequent material jamming in the filament pulling mechanism, and the proper control parameters for printing thin diaphragms are well understood.

All 3D models including test structures and the microfluidic device reported in this paper were designed and modeled using SolidWorks (SolidWorks Corp., Waltham, MA). The design files were exported as STL files, and the devices were fabricated using a low-cost extrusion-based 3D printer, the Wanhao duplicator 4X printer (Jinhua Wanhao Ltd., China). The open-source 3D printing program ReplicatorG was used to drive the printer. The 3D printing material NinjaFlex was purchased in filament form with a nominal diameter of 1.75 mm. According to the manufacturer's user manual, the duplicator 4X printer has a positional accuracy of 11 μm in the x and y directions and 2.5 μm in the z direction. The highest layer resolution is 100 μm . The diameter of the printer nozzle is 0.4 mm.

We conducted a series of calibration tests to determine the optimized control parameters for printing NinjaFlex microfluidic systems with flexible diaphragms of similar dimensions as our PDMS microfluidic devices (Yao et al. 2013b). In the design file, the width of the microchannel is 600 μm . We printed more than 50 microchannel samples, and their average width was determined to be $600 \pm 20 \mu\text{m}$. In the design file, the thickness of the diaphragm is 400 μm . Based on multiple samples, the average width of the 3D-printed diaphragm was $400 \mu\text{m} \pm 15 \mu\text{m}$. The diaphragms were printed without a support material since it is almost impossible to strip the material afterward owing to the small openings of the microfluidic system. The control parameters of the ReplicatorG include object infill, number of shells, layer height, print temperature, and feedrate. The object infill determines the density of the printed object, as demonstrated in Fig. 2. Theoretically, a solid object can be obtained by setting this parameter at 100%. For our microfluidic devices, the object fill is set at 100% to avoid defects such as small holes in the printed diaphragms.

The number of shell defines the outer structure of the printed object. It is not a crucial parameter for the microfluidic system because the system is printed as a solid object. We set this parameter at 1. The layer height determines both the thickness and flatness of each printed layer. In extrusion-based printing, the layer height is usually kept low to minimize the surface roughness of each layer. However, a low layer height also leads to a prohibitively long

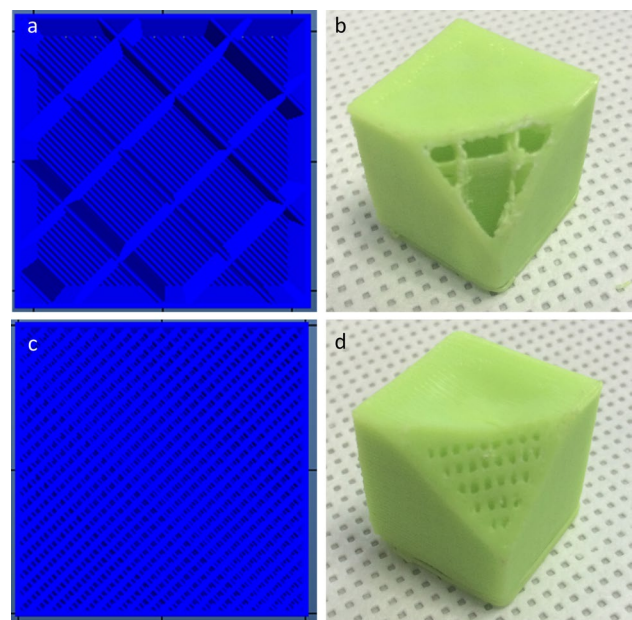


Fig. 2 3D-printed objects with different object infill percentages. **a** Surface at 10% infill. **b** A 20 mm \times 20 mm \times 20 mm cube at 10% infill. **c** Surface at 50% infill. **d** A 20 mm \times 20 mm \times 20 mm cube at 50% infill

printing time. We selected a layer height of 0.2 mm as a compromise between surface roughness and print time.

Perhaps the most critical control parameters for printing NinjaFlex are the print temperature and feedrate. The print temperature dictates the material bonding performance, material flow rate, and extrusion width. If the temperature is too low, the material extrudes with high viscosity which leads to overly thin print layers. On the other hand, if the temperature is too high, the material extrudes with high liquidity which tends to cause deformation in the printed object. We determined the optimized print temperature for NinjaFlex to be between 210 and 220 $^{\circ}\text{C}$.

The feedrate is the traversing speed of the printer nozzle as it extrudes material. The feedrate for stiff materials such as ABS and PLA is generally set at 20–50 mm/s. For NinjaFlex, the feedrate is set at a lower number since NinjaFlex is flexible and therefore prone to clogging at the print nozzle at the same feedrate range. In addition, if the feedrate is too high, the extruded NinjaFlex is thinned out rapidly by the traversing nozzle. As shown in Fig. 3, small holes can be found on a 3D-printed NinjaFlex diaphragm when the feedrate is set at a high 40 mm/s. We determined the optimized feedrate for NinjaFlex to be 5 mm/s.

Another control parameter that can also affect the quality of the printed object is the plate temperature. We set this temperature at 40 $^{\circ}\text{C}$ to minimize edge warping in the printed device. Using the control parameters described above, the average print time for a complete NinjaFlex

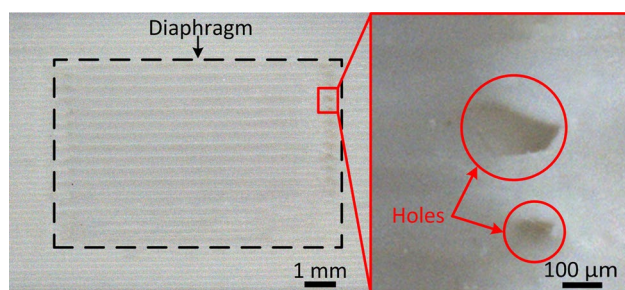


Fig. 3 Small holes in 3D-printed NinjaFlex diaphragm when the feedrate is set at 40 mm/s

microfluidic system is about 5 h. Since no support material is used, the microfluidic system is ready for testing as soon as the printing process is completed.

3 Results and discussion

3.1 Young's modulus

In order to properly design the dimensions of the flexible diaphragms in the NinjaFlex microfluidic system, we conducted mechanical deflection experiments to determine the Young's modulus of NinjaFlex at room temperature. In these experiments, the peak deflection of a circular NinjaFlex plate was measured at different values of applied air pressure. The Young's modulus E was then determined by curve fitting the experimental result with the theoretical circular plate deflection equation:

$$\frac{pr^4}{Et^2} = \frac{5.33}{1-\nu^2} \cdot \frac{y}{t} + \frac{2.6}{1-\nu^2} \cdot \left(\frac{y}{t}\right)^3$$

where p is the pressure on the plate, r is the plate radius, t is the plate thickness, ν is the Poisson's ratio, and y is the peak deflection of the plate (Young and Budynas 2002). We used the commonly cited TPE ν value of 0.499 in our calculations (Rose et al. 1987). Figure 4a demonstrates the design of the NinjaFlex test structure used to determine E . It consists of a thick-walled pneumatic air chamber with a thin circular plate at the top. The length, width, and height of the air chamber are 30, 30, and 13.6 mm, respectively. Figure 4b shows that the thicknesses of the side and bottom walls are 3 and 4 mm. The radius and thickness of the plate are 12 and 1.6 mm. The sidewall of the air chamber is designed to be much thicker than the plate so that the wall does not deform significantly when compressed air is applied to the chamber. Figure 4c demonstrates a typical plate deflection, and Fig. 4d demonstrates the relationship between applied air pressure and peak plate deflection.

The curve fitting result yields a Young's modulus of approximately 16.35 MPa for NinjaFlex. This is much

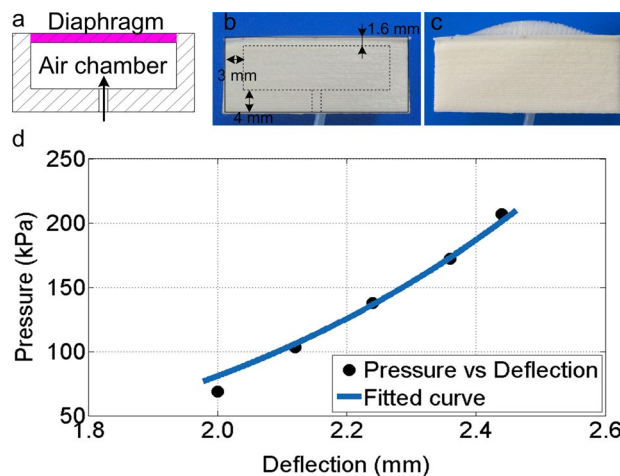


Fig. 4 Young's modulus measurement. **a** Design of NinjaFlex test structure. **b** Test structure at 0 psi applied pressure. **c** Plate deflection at 30 psi; **d** relationship between applied pressure and peak deflection

smaller than the most commonly used extrusion printing materials such as ABS (Young's modulus ~2–4 GPa). The average Young's modulus of PDMS is approximately 2 MPa depending on the ratio of the elastomer base and curing agent (Wang 2011). The Young's modulus of NinjaFlex is therefore approximately eight times higher than that of PDMS.

3.2 Water absorption and surface hydrophobicity

For microfluidic devices, it is always desirable to minimize the absorption of the sample fluid and assay molecules into the sidewalls of the microfluidic channels in order to achieve a high degree of repeatability and consistency in the test result (Wang et al. 2012). We measured the water absorption properties of NinjaFlex and compared it with those of cured PDMS. Due to the nature of extrusion-based 3D printing, small gaps exist between the fibrous material in a printed layer and these gaps provide an avenue for fluid to be absorbed into the printed material. To fill the gaps, the printer nozzle traverses at an offsetted grid from layer to layer. However, small holes can still exist in the bottom surface of the printed object, making the surface slightly porous. The average size of the holes is approximately 0.01 mm^2 . The hole size becomes progressively smaller as the number of printed layers increases and the object becomes thicker. The holes usually disappear completely when the print thickness reaches 1 mm. We printed all of our microfluidic systems with a bottom layer thickness of over 1 mm to minimize water absorption into the system.

The water absorption test monitors the change in weight of three different NinjaFlex samples (weighing at 3.4, 8.6, and 16.6 g when dry) as they are immersed in DI water.

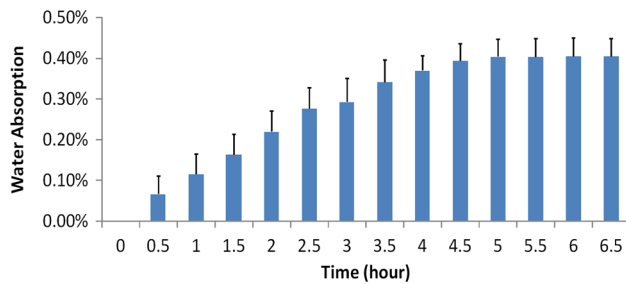


Fig. 5 Result of NinjaFlex water absorption test. The result shown here is the combined results from three NinjaFlex samples weighing at 3.4 g, 8.6 g, and 16.6 g, respectively, when dry

During the test, the DI water container is sealed to prevent water loss due to evaporation. The weight of the three immersed samples is measured every 0.5 h.

As shown in Fig. 5, the weight of the NinjaFlex samples increases continuously during the first 4 h and then remains mostly constant afterward. Among the samples tested, the water absorption of the largest sample is consistently the lowest. At steady state, the water absorption of the 3.4, 8.6, and 16.6 g samples is approximately 0.47, 0.38, and 0.36%, respectively. The maximum amount of water absorbed is therefore 0.47% of the dry sample weight. This is higher than the water absorbance property of PDMS which is approximately 0.1% (Ping et al. 2001).

An equally important physiochemical property of NinjaFlex for microfluidic applications is whether the printed surface is hydrophobic or hydrophilic. Freshly cured PDMS surface is hydrophobic, which sometimes prevents PDMS microfluidic channels from being properly wetted during testing. We tested the surface hydrophobicity of NinjaFlex by depositing a 30- μ L drop of DI water mixed with yellow ink on a 3D-printed microfluidic device with a pipette and then measuring the static contact angle of the drop. In order to minimize measurement error, the test was repeated at three different locations on each surface tested. The contact angle measurements were observed to stay unchanged for over 20 h. During the 20-h test time, we deposited a new 30- μ L drop of DI water mixed with yellow ink every time we measured the contact angle. An optical microscope (Zoom 6000, Navitar Inc., USA) was used to record the contact angle pictures, and Adobe Photoshop CS 6 was used to measure the angles. As shown in Fig. 6, the average contact angle of the side surface is 51.9° with a standard deviation of 0.06°. The average contact angle of the top surface is 53.3° with a standard deviation of 0.15°. This result implies that a printed NinjaFlex surface is hydrophilic, while the surface of native PDMS is hydrophobic with a water contact angle of between 95 and 110° (Lawton et al. 2005). PDMS can become hydrophilic after oxidation with a contact angle of 50–60° (Lawton et al.

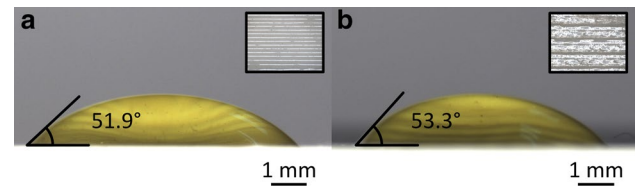


Fig. 6 Water contact angle of NinjaFlex surfaces. **a** Water contact angle of side surface. Inset shows a magnified side surface. **b** Water contact angle of top surface. Inset shows a magnified top surface

2005). A 3D-printed NinjaFlex surface achieves this level of hydrophilicity without chemical processing. We measured the surface roughness at five different locations on the printed surface using a compact roughness measuring instrument (MarSurf PS10, Mahr Federal Inc., Germany). The surface roughness Ra (arithmetical mean deviation of the surface) is 25.10 μ m, and the standard deviation is 7.12 μ m.

3.3 Biocompatibility

The biocompatibility of NinjaFlex was assessed by testing its cytocompatibility in a printed NinjaFlex well plate (Fig. 7a, inset) as well as on a printed NinjaFlex surface according to the direct contact method as per ISO-10993-5 guideline (Iso and Standard 2009) with some modifications. A Corning® 96-well culture plate (Corning Inc., Corning, NY, USA) and a PDMS surface were used as controls, respectively. In the well plates, cell viability and proliferation were monitored for 10 days using CellTiter 96® AQueous One Solution Cell Proliferation Assay (Promega, Madison, WI, USA) with mammalian mouse fibroblast cell line and ATCC® CCL-1™ (American Type Culture Collection [ATCC], Manassas, VA, USA) according to the specifications by Promega and ATCC. On the surfaces, the cell proliferation was observed for 2 days under an inverted light microscope with human embryonic kidney cell line, ATCC® CRL-1573™, according to the specifications by ATCC. All experiments were performed in compliance with guidelines set by the Institutional Biosafety Committee (IBC) at the University of Arkansas and approved by the IBC. Briefly, the CCL-1 cell line was cultured in Dulbecco's modified Eagle's medium supplemented with 10% fetal bovine serum at 37 °C and 5% CO₂. After being cultured, the CCL-1 cells were trypsinized, the cell suspension was centrifuged at 200 \times g for 3 min, and the cells were resuspended in culture medium at a density of 1 \times 10⁵ cells/mL. Both the control (*i.e.*, a 96-well culture plate) and the printed NinjaFlex well plates were seeded with 100 μ L of the cell suspension (*i.e.*, 1 \times 10⁴ cells/well). After a 24-h incubation at 37 °C and 5% CO₂, the spent culture medium was replaced with an equal volume

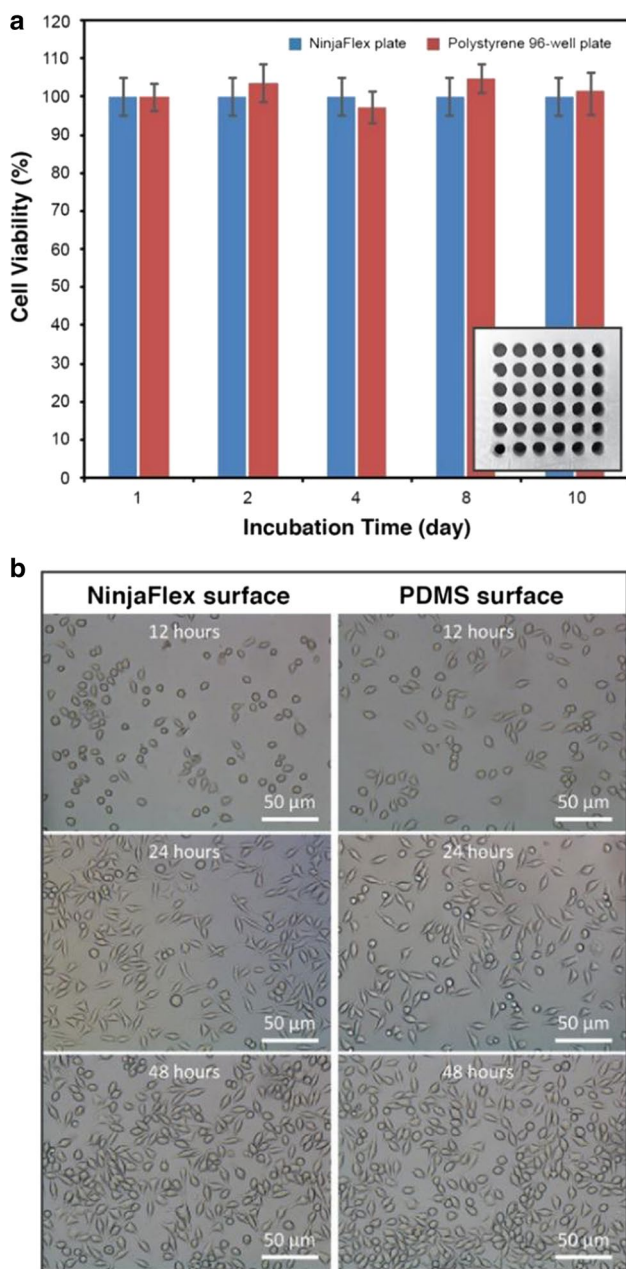


Fig. 7 Biocompatibility studies of NinjaFlex. **a** Cell viability and proliferation assays. Cell viability and proliferation were monitored for 10 days using CellTiter 96[®] AQ_{ueous} One Solution Cell Proliferation Assay (Promega, Madison, WI, USA) with mammalian mouse fibroblast cell line (ATCC[®] CCL-1[™], American Type Culture Collection, Manassa, VA, USA). Note that all experiments were performed three times in triplets, and the average at each time interval has been shown as cell-viability percentage of the sample in the NinjaFlex well plate in comparison with the control sample in the polystyrene 96-well plate. The control at each time interval was considered as 100% viable. *Inset* A printed NinjaFlex well plate with the dimension of: D (diameter) = 6.5 mm and H (height) = 12.2 mm (i.e., total volume of 405 μ L). **b** Cell adhesion and proliferation tests. Cell phenotypes and proliferations on the NinjaFlex and PDMS surfaces were monitored during incubation for 2 days under an inverted light microscope with human embryonic kidney cell line (ATCC[®] CRL-1573[™])

(100 μ L) of the culture medium and the well plates were incubated for 10 days at 37 °C and 5% CO₂. After incubation, the cell proliferation assay was performed and the cell-viability profile was assessed by colorimetric absorbance at 490 nm using a DU-800 ultraviolet/visible/NIR (UV/VIS/NIR) spectrophotometer (Beckman Coulter Inc., Fullerton, CA, USA). The extended incubation time of 10 days was chosen to allow sufficient time for NinjaFlex to influence, if any, the cell viability.

The CRL-1573 cell line was cultured in Eagle's minimum essential medium supplemented with 10% fetal bovine serum at 37 °C and 5% CO₂. The printed NinjaFlex surface and PDMS surface were placed on separate cell culture petri dishes (Corning Inc., Corning, NY, USA) containing the culture medium. The cells were seeded in the culture dishes and incubated at 37 °C and 5% CO₂. The cell morphology and proliferation on each surface were monitored during incubation for 2 days under an inverted light microscope (Axiovert 40 CFL, Carl Zeiss, Inc., Germany) equipped with a Zeiss AxioCam MRc5.

If the NinjaFlex microfluidic devices are to be used for biological and biomedical purposes, the material's biocompatibility will be an important factor for consideration. While PDMS is known to be biocompatible (Bélanger and Marois 2001; Zhou et al. 2010) (Zhang et al. 2013), no such information is available for NinjaFlex. We examined the cytocompatibility of NinjaFlex by not only monitoring the cell viability and proliferation in a printed NinjaFlex well plate (Fig. 7a, inset) with a commercial polystyrene 96-well culture plate as a control, but also observing the cell morphology and proliferation on a printed NinjaFlex surface with a PDMS surface as a control. Cell viability and proliferation assays revealed that NinjaFlex maintained cell viabilities nearly identical to the cultures on the commercial polystyrene well plate, implying no apparent adverse toxicity effects on live cells after their exposure to NinjaFlex for 10 days. The cell adhesion and proliferation tests on a printed NinjaFlex surface for over 2 days indicated no marked changes in the attachment and proliferation of cells as compared to those on the PDMS surface (Fig. 7b). The NinjaFlex surface also sustained cell phenotypes nearly identical to those on the PDMS surface. The results clearly suggest the biocompatibility of NinjaFlex with minimal cytotoxicity, therefore enabling their uses for biological and biomedical applications.

3.4 Design and fabrication of 3D-printed peristaltic micropump

Based on an existing PDMS design, we developed a 3D-printed NinjaFlex peristaltic micropump using movable diaphragms as actuators. As demonstrated in Fig. 8a,

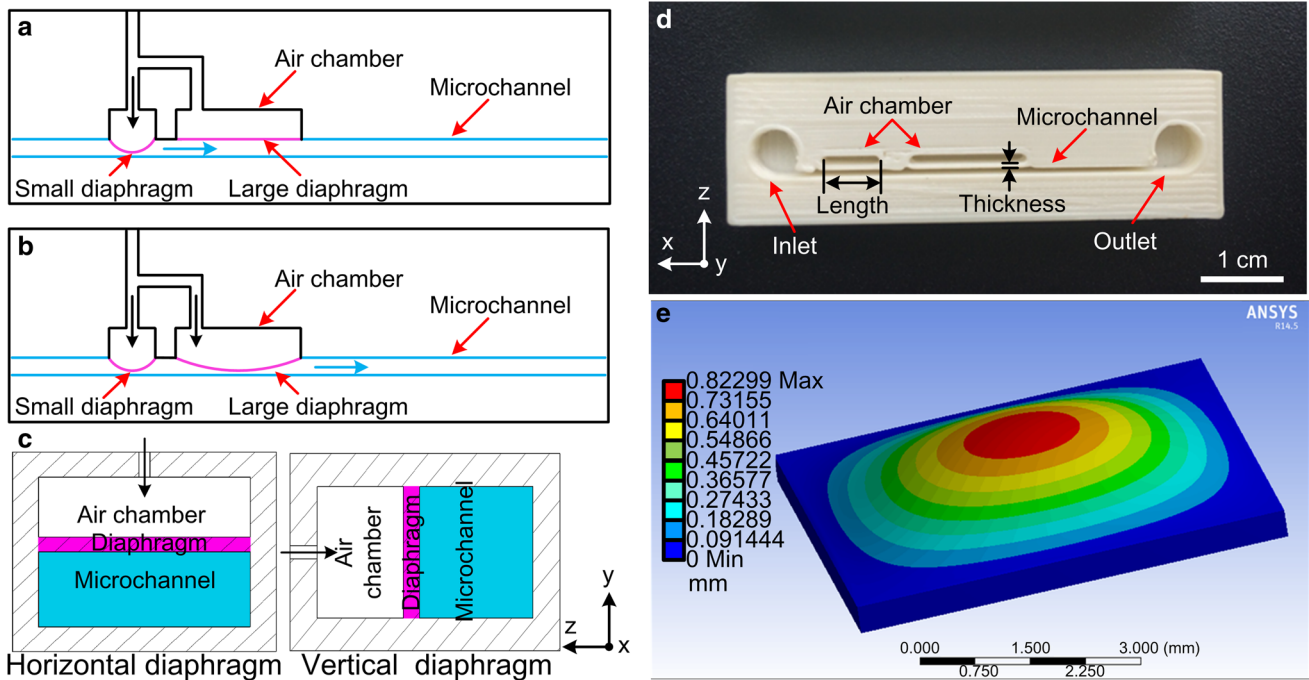


Fig. 8 Design of the 3D-printed NinjaFlex peristaltic micropump. **a** As air pressure is applied to the common air chamber inlet, the small diaphragm deflects first and cuts off the backflow. **b** The large diaphragm deflects next and squeezes the fluid moving forward. **c** Schematic diagrams of the horizontal and vertical diaphragm configura-

tions. X is the streamwise direction. **d** Cutout demonstration of the 3D-printed micropump. **e** ANSYS simulation of small diaphragm deflection at 10 psi. The color heat map shows that the maximum deflection is about 0.82 mm

b, two diaphragms, one small and one large, are deflected sequentially by an external compressed air source to pump sample fluid in a microchannel. The small diaphragm performs the function of a check valve, while the large diaphragm moves the fluid. Two possible diaphragm configurations can be used to generate this peristaltic motion: vertical and horizontal (Fig. 8c). In the horizontal configuration, the diaphragms are oriented in the $x-z$ plane, while in the vertical configuration, the diaphragms are in the $x-y$ plane. Horizontal diaphragm can be considered as a movable ceiling of the microchannel, while vertical diaphragm behaves as a movable sidewall. In PDMS microfluidic devices, the diaphragms are mostly oriented in the horizontal direction due to limitations of the micromolding fabrication process (Sundararajan et al. 2005). It is also difficult to attach a capping piece to the thin vertical sidewall of a PDMS device since only a small area is available for bonding. Extrusion-based 3D printing is capable of fabricating both vertical and horizontal diaphragms. 3D-printed devices, especially those printed in TPE, therefore provide a new opportunity to fully explore the advantages of vertical diaphragms without the need for a cumbersome material bonding process. In addition, 3D printing can fabricate a capped-off microfluidic device in one single step, while PDMS devices usually require a separate capping process to seal off the

microchannels. In general, 3D printing allows significantly more design freedom in terms of the incorporation of three-dimensional features into the microfluidic system than PDMS micromolding, which is mostly a two-dimensional planar process. Finally, the inlets and outlets of a 3D-printed microfluidic system can be located on the sidewalls of the device, which is difficult to achieve in a PDMS device. This option frees up the top surface of the device and provides a cleaner area for optical observation of the microchannel flow if needed. In extrusion-based 3D printing, special care must be taken when fabricating overhanging structures to avoid structural sagging during the printing process. Theoretically, a second printing material can be used as a support material under the diaphragms to be stripped away by a liquid solvent when the printing process is complete. For the peristaltic micropump, this proves to be difficult since the openings to the support material are very small and the time required to completely dissolve the support material can be extremely long. We therefore elected to print the NinjaFlex diaphragms in the vertical configuration. A cutout demonstration of the 3D-printed NinjaFlex micropump is shown in Fig. 8d. The major components of the micropump include a microfluidic channel, two vertical diaphragms, and a pair of pneumatic air chambers with a common compressed air inlet. The thickness and width of the diaphragms are 0.4 and

5 mm, respectively. The lengths of the small and large diaphragms are 6 and 12 mm, respectively. The width of the microfluidic channel is 0.6 mm. It is 40 mm long from the inlet to the outlet. When compressed air is introduced to the air chambers, the small diaphragm deflects first due a smaller volume capacity, followed by the large diaphragm after short delay. To generate a continuous flow, periodic air pulses are used to create periodic, sequential deflections in the diaphragms, which in turn leads to peristaltic pumping in the microfluidic channel. Using the experimentally determined Young's modulus, we conducted ANSYS simulations to obtain the deformation characteristics of the NinjaFlex diaphragms. Here, the diaphragms are treated as thin, isotropic, rectangular plates with fixed boundaries. As shown in Fig. 8e, the simulations predict a peak deflection of 0.82 mm in the small diaphragm (6 mm × 5 mm × 0.4 mm) at an applied pressure of 10 psi. This deflection is larger than the width of the microfluidic channel, thus ensuring the proper functioning of the small diaphragm as a check valve.

3.5 Micropump flow rate

The control system for measuring the flow rate of the 3D-printed micropump is shown in Fig. 9. It consists of a compressed air source, a rectangular-pulse signal generator, twelve individually controlled electromagnetic valves (EMVs, S070 M-5BG-32, SMC Inc., Tokyo, Japan), and the micropump. The air pulses from the EMVs are delivered to the inlet port of the air chamber of the micropump through a 1.8-mm (diameter) PTFE (polytetrafluoroethylene) tubing. The power of the compressed air source is about 10 W. The power of each electromagnetic valves is about 0.35 W. Each micropump requires one EMV for actuation. The response time of the EMV is 3 ms ON/OFF according to the user manual. The signal generator outputs the rectangular pulses that control the opening and closing of the electromagnetic valves at a predetermined frequency. The peak pressure of the compressed air pulses delivered to the micropump from the EMVs is controlled by a pressure regulator. The inlet and outlet of the micropump are

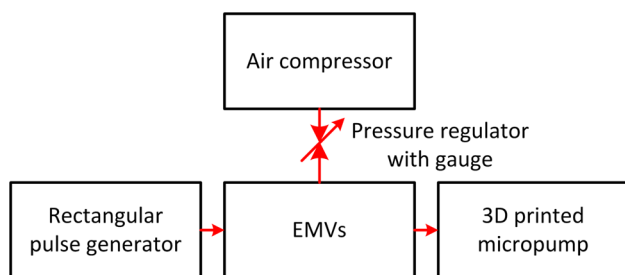


Fig. 9 Schematic diagram of the control system for measuring the flow rate of 3D-printed micropump

connected to open reservoirs filled with a red dye solution. A Tygon tubing is connected to the outlet reservoir, and the micropump's flow rate is estimated by multiplying the advancing speed of the red dye in the Tygon tubing by the cross-sectional area of the tubing (1/8" diameter). During flow rate measurements, the liquid level of the inlet and outlet reservoirs is set to be identical so that no hydrostatic pressure difference exists between the two reservoirs.

We measured the peak displacement of the diaphragm (12 mm × 5 mm) versus applied pressure from 10 to 95 psi. The peak displacement ranges from 406 to 2894 μm, and the diaphragm did not break at 95 psi. The maximum actuation pressure we used for the micropump is usually 20 psi because the displacement of the diaphragm at this pressure is larger than the microchannel width, thus ensuring the proper functioning of the diaphragm as a check valve.

The pressure range for the micropump was selected based on the experimentally determined diaphragm deflection characteristics as well as those obtained from COMSOL simulations. Based on this information, we evaluated the flow rate performance of the 3D-printed micropump by varying the frequency and pressure of the periodic compressed air pulses. The micropump was tested at three different peak pressure levels of 10, 15, and 20 psi. At each peak pressure, the frequency was varied from 5 to 10 Hz at 1-Hz intervals. Figure 10 shows the flow rates measured at different pressure and frequency values.

At each pressure, the flow rate follows a bell-shaped relationship with frequency, which is consistent with the

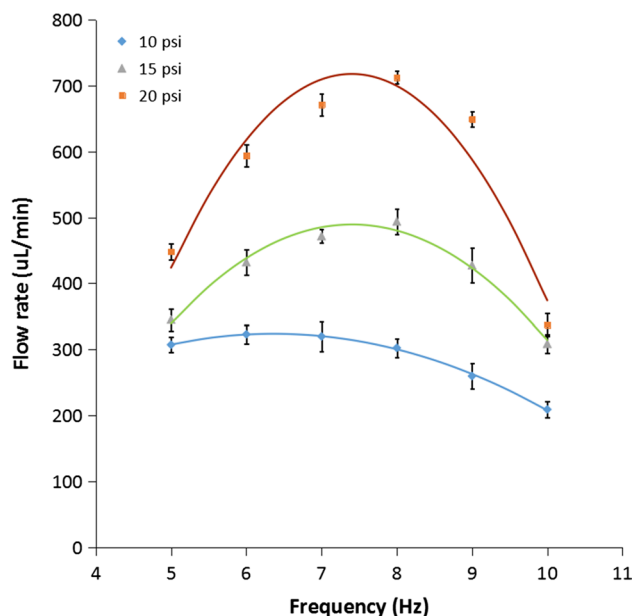


Fig. 10 Flow rate of 3D-printed micropump versus compressed air pressure and frequency. Each flow rate measurement was repeated three times for every frequency

behavior of our PDMS peristaltic micropump (Yao et al. 2013b). A peak flow rate can be identified at each driving pressure, and the level of the peak flow rate increases with increasing pressure. The frequency at which the peak flow rate is observed is referred to as the optimal frequency. A maximum flow rate of 712.56 $\mu\text{L}/\text{min}$ is achieved at 8 Hz and 20 psi. When the pressure is reduced to 15 psi, the maximum flow rate drops to 494.04 $\mu\text{L}/\text{min}$. These flow rate values are in the same range as that of the PDMS micropump. Figure 11 shows the relationship between the measured flow rate of the micropump at 7-Hz actuation frequency and the backward hydraulic pressure.

3.6 3D-printed micromixer

Rapid and efficient mixing plays a significant role in a variety of microfluidic-based biomedical applications including insulin detection (Yao et al. 2016), glucose-catalyst reactions detection (Kim et al. 2005), and virus or pathogen detection (Jung et al. 2011; Lai et al. 2014). Based on the design of the 3D-printed micropump, we developed a diaphragm-driven micromixer to perform active mixing of sample fluids. As demonstrated in Figs. 12a and 12b, the micromixer consists of two inlets and one outlet. Two 5 mm \times 4.4 mm and 0.4 mm thick diaphragms (marked in purple) form the internal sidewalls of a mixing chamber (6 mm \times 6 mm \times 7 mm). Similar to the micropump, the diaphragms are deflected by externally supplied compressed air and active mixing is achieved by in-phase or out-of-phase periodic diaphragm movement. Notice the compressed air inlets are located on the external sidewalls of the micromixer. Dilution experiments were conducted to evaluate the performance of the micromixer. In these experiments, colorless DI water and a red dye solution were slowly injected into the mixing chamber through the fluid inlets, and their mixing characteristics were monitored over time. At the

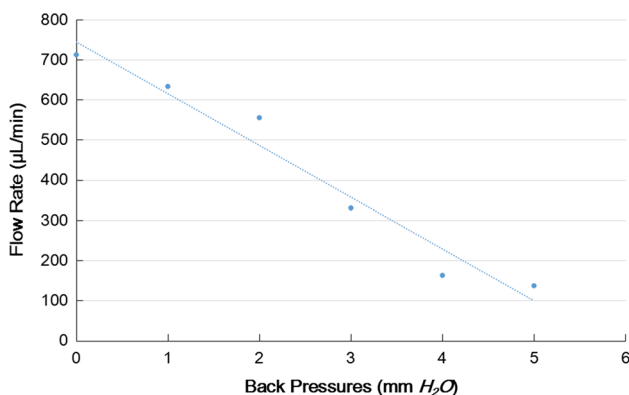


Fig. 11 Measured flow rate of the micropump versus backward hydraulic pressure

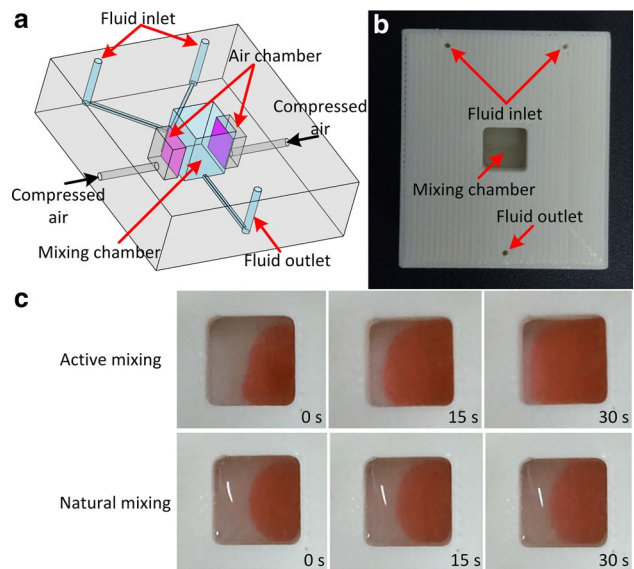


Fig. 12 3D-printed NinjaFlex micromixer. **a** Schematics of the micromixer. **b** Top view of the 3D-printed micromixer used in the dilution experiments. **c** Time sequence photographs of natural and active mixing

beginning of each test, the dye and water were added to the mixing chamber until a clear interface appeared between the two fluids. An optical microscope was used to acquire the images of the mixing process. A MATLAB program was used to analyze the gray level of these images to determine the mixing efficiency I_g defined as:

$$I_g = 1 - \frac{1}{C} \sqrt{\frac{\sum [C(y) - \bar{C}]^2}{N}}$$

where N is the number of pixels. $C(y)$ is the gray level of a pixel, and $\bar{C} = \sum C(y)/N$. We define the mixing time as the time when the mixing efficiency reaches 80%. Figure 12c shows the difference between natural (unassisted) mixing and active mixing where the diaphragms are deflected in phase by compressed air at 10 Hz and 10 psi. Diaphragm-induced fluid advection in the mixing chamber accelerates the water-dye mixing process and enhances the mixing efficiency. The mixing time of active mixing in the micromixer is 38 s, while that of the unassisted mixing is 233 s. Active mixing reduces the mixing time by about 80%. It has been previously reported that pneumatic micromixers can reduce the mixing time by about 93% (Kong and Salin 2012).

3.7 Insulin detection using 3D-printed microfluidic system

We integrated the 3D-printed micropump and micromixer designs into a monolithic microfluidic system

and demonstrated its effectiveness in the rapid detection of insulin concentration through a chemiluminescence immunoassay.

Experiments for determining the insulin detection performance of the 3D-printed microfluidic system are conducted in a custom-designed automation and optical detection system previously developed for testing our PDMS microfluidic systems. As shown in Fig. 13a, this system consists of a photomultiplier tube (CR105-01, Hamamatsu, Hamamatsu City, Japan) to quantify the chemiluminescence signal. It is also equipped with a mini-air compressor (D730A-23-01, Hargraves Technology Mooresville, NC, USA), a pressure regulator (IR2000-02, SNS, Zhengjiang, China), a signal generator (S3C2440, Samsung, Seoul, South Korea), 12 electromagnetic valves (S070 M-5BG-32, SMC Inc., Tokyo, Japan), an electromagnet (TAU-0730, Kendrion, Villingen-Schwenningen, Germany), and a stepper motor (N20, Arduino, Ivrea, Italy). The PDMS device shown in Fig. 13b is fabricated from two PDMS layers and one glass layer using micromolding and oxygen plasma bonding. It consists of five individually controlled pneumatic micropumps and one micromixer at the center.

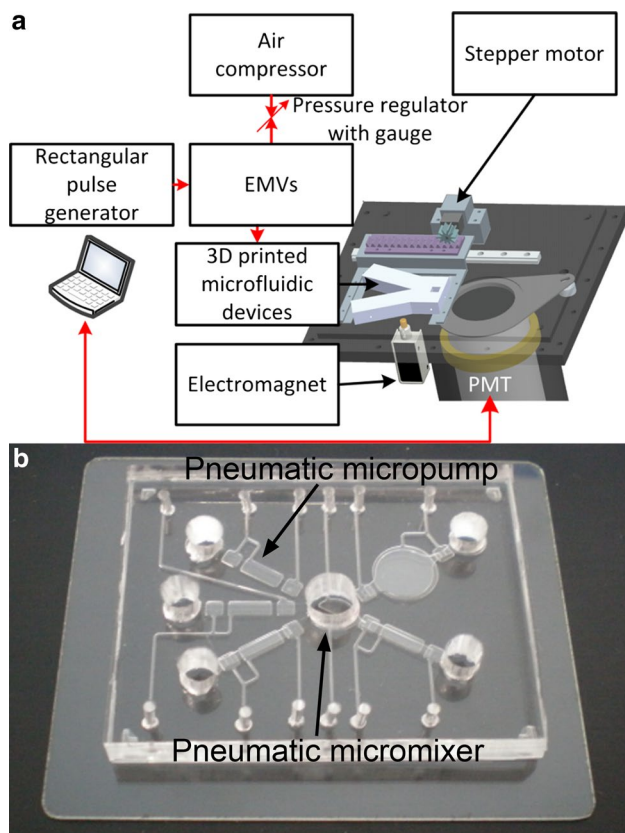


Fig. 13 **a** Schematic diagram of the insulin detection system and **b** photograph of a PDMS microfluidic device designed for insulin detection using the same setup shown in (a)

The height and width of the microchannel are 250 and 1200 μm , respectively. Both the 3D-printed device and the PDMS device developed by our group for insulin detection utilize diaphragm-based pneumatic actuation for pumping and mixing. They are also operated in similar pressure and frequency ranges.

As demonstrated in Fig. 14a, the 3D-printed microfluidic system consists of two micropumps and one micromixer. The micropumps enable controlled delivery of sample fluids from two separate inlets to the micromixer where the immunoassay is carried out. Figure 14b illustrates the biological protocol of the immunoassay. The electromagnet is programmed to retain the magnetic microparticles in the sample fluid during the wash steps of the immunoassay (steps C and F in Fig. 14b). The stepper motor is utilized to move the microfluidic device to the optical detection zone to record the chemiluminescent light in the last step of the immunoassay (step H in Fig. 14b). To minimize the interference from unwanted light sources, the 3D-printed microfluidic system is kept inside a custom-designed black box during the experiments and 12 Teflon tubes are used to supply the required air pulses from an external source. The key steps of the chemiluminescence immunoassay for insulin detection are as follows. First, superparamagnetic microparticles coated with insulin antibodies ($\sim 30 \mu\text{g}/\text{mL}$, $40 \mu\text{L}$) are used to capture the target insulin antigens ($20 \mu\text{L}$) through specific binding in the micromixer (steps A and B in Fig. 14b). Second, the superparamagnetic microparticles with target insulin antigens are held down by the electromagnet, while the interference substances are washed away (step C in Fig. 14b). Third, insulin antibodies labeled with acridinium ester (AE; $\sim 0.25 \mu\text{g}/\text{mL}$, $40 \mu\text{L}$) are pumped into the mixer to bind to the insulin antigens on the microparticles, forming a sandwich complex (steps D and E in Fig. 14b). With the electromagnet holding down the complex, the overdose AE-labeled insulin antibodies are removed through a washing step (step F in Fig. 14b). Fourth, the first developing solution (3% H_2O_2 solution containing 0.1 N HNO_3 , $40 \mu\text{L}$) is pumped into the mixer and allowed to incubate with the microparticles for 1 min (step G in Fig. 14b), followed by a second developing solution (1.5 N NaOH solution containing 2% Triton X-100, $40 \mu\text{L}$) delivered into the mixer at a high flow rate to initiate the chemiluminescence reaction (step H in Fig. 14b). Reagents are transported at a flow rate of $712 \mu\text{L}/\text{min}$. The diaphragms of the mixing chamber are actuated at a driving frequency of 10 Hz and an applied pressure of 10 psi. The entire insulin detection assay requires approximately 15 min. This protocol was previously developed by our group for a PDMS pneumatic microfluidic system (Yao et al. 2016). Figure 14c demonstrates the insulin detection result. The inset provides the timeline of a typical light intensity measurement of the

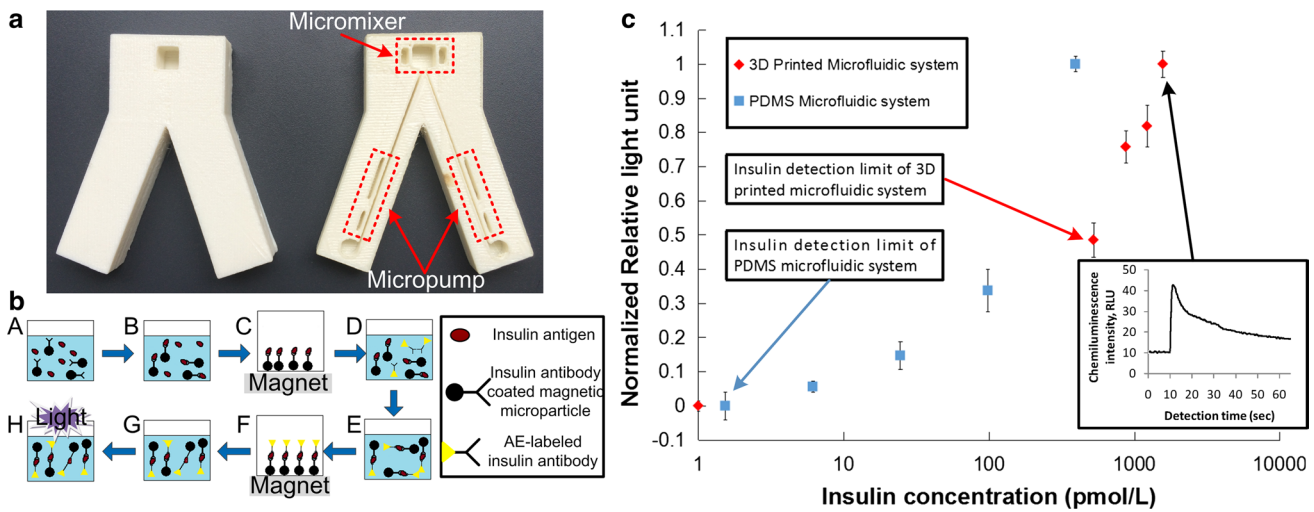


Fig. 14 Insulin detection by a 3D-printed integrated microfluidic system. **a** Photograph of the 3D-printed device and a dissected device showing the internal structure. **b** An illustration of the biological protocol for insulin detection using a chemiluminescence immunoas-

say. **c** Result of insulin detection showing a side-by-side comparison between 3D-printed system and similarly designed PDMS system. The *inset* demonstrates a typical light generation trend of the chemiluminescence reaction

chemiluminescence reaction in the micromixer chamber. It shows that the light intensity reaches a peak value rapidly and then gradually declines back to the baseline. The peak value is directly proportional to the insulin concentration of the sample. The error bars in the figure represent the standard deviations of the measured light intensities. The standard deviations from the lowest to the highest concentrations are 0.014, 0.050, 0.046, 0.061, and 0.038, respectively. Three assays were performed for each concentration. Matrix spiking was used to evaluate the accuracy of the insulin detection method. The test was performed by adding the insulin standard solution of known concentration to the insulin sample and then measuring the concentration of the matrix spiked sample. Both the spiked and unspiked samples were analyzed in the 3D-printed microfluidic system. An intermediate value (1218 pM) between the detection limit and the highest insulin concentration tested was chosen to be the spiking level. The concentration of the spiking solution was 358 pM. Based on the results, the percent recovery of the spike was determined to be about 82.6%, which we believe is a satisfactory level for the current development stage of the 3D-printed microfluidic system. We used the same 3D-printed device in multiple test runs. After each test run, the device is washed by PBS and then DI water before being used again. As shown in Fig. 14c, the 3D-printed system and the PDMS system are tested in two different insulin concentration ranges due to differences in their detection limits. However, with the exception of the measurements recorded near 500 pM, the PDMS and 3D-printed results appear to form a consistent light intensity trend with respect to the insulin concentration. We therefore believe that the sensitivity trend of

the 3D-printed system will be very similar to that of the PDMS system if its detection limit is reduced. Quantitatively, the insulin detection limit of the 3D-printed device is 522.4 pM, while that of the PDMS device is 6.1 pM. Further optimization of the structural design and actuation parameters of the 3D-printed device should reduce the detection limit. For example, as described in a previous article published by our group, increasing the micropump flow rate can lead to a more efficient chemiluminescence process and consequently a reduction in the detection limit (Yao et al. 2016). In addition, reducing the dimensions of the microchannel can also increase the flow rate and therefore reduce the detection limit. As a reference point, the current detection limit of commercial immunoassay systems for insulin detection is about 3.5 pM (Yao et al. 2016).

4 Conclusions

In this paper, we reported the development of a 3D-printed microfluidic system using a commercially available TPE as the structural material. The microfluidic system was designed using SolidWorks and fabricated directly from the design file by a low-cost extrusion-based 3D printer. No additional bonding or curing step is required by the fabrication process, and the device is ready for use as soon as the print job is complete. The Young’s modulus of the TPE is about eight times higher than that of PDMS, but much lower than the commonly used printing materials such as ABS, making TPE a good choice for printing PDMS-like microfluidic devices. TPE is also demonstrated

to be biocompatible with minimal cytotoxicity. The printed TPE surface is hydrophilic which allows easy wetting of the printed microchannels. The performance of TPE-based 3D-printed pneumatic micropump and micromixer was experimentally investigated to determine the flow rate and mixing characteristics. When applied in a chemiluminescence immunoassay for determining insulin concentration, an integrated TPE microfluidic system exhibits a similar sensitivity trend as a microfabricated PDMS pneumatic microfluidic system. Additional optimization work will be required to improve the insulin detection limit of the 3D-printed system as well as a number of material and system-related issues. For example, the TPE NinjaFlex is only semitransparent, which can cause difficulties in optical detection. The micromixer discussed in this paper is intentionally designed to be open on the top due to this limitation. In addition, the printed TPE surface is rougher than molded PDMS. This can cause unwanted trapping of sample materials in bead-based assays. Nonetheless, the availability of a structure material with similar properties to PDMS and the tremendous shortening of the turnaround time for new designs should make extrusion-based 3D printing a very attractive alternative for the design and fabrication of microfluidic systems. Recent development in syringe-based extrusion printing has shown promises in printing nm-wide polymer lines resulting in an exceptionally smooth printed surface. We therefore believe the issue of surface roughness for extrusion-based 3D-printed microfluidic systems can be significantly improved in the near future.

Acknowledgements This paper is supported by the National Natural Science Foundation of China (Grant No. 61573339) and the CAS FEA International Partnership Program for Creative Research Teams. The authors would like to thank Mrs. E.M. Martin and J. Hockman for their assistance with cell cultures and sample preparation.

References

- Au AK, Bhattacharjee N, Horowitz LF, Chang TC, Folch A (2015) 3D-printed microfluidic automation. *Lab Chip* 15:1934–1941. doi:10.1039/c5lc00126a
- Bélanger MC, Marois Y (2001) Hemocompatibility, biocompatibility, inflammatory and in vivo studies of primary reference materials low density polyethylene and polydimethylsiloxane: a review. *J Biomed Mater Res* 58:467–477
- Holden G (2000) Understanding thermoplastic elastomers. Hanser Verlag, Munich
- Iso B, Standard B (2009) Biological evaluation of medical devices. Part 1:10993
- Jung JH, Kim G-Y, Seo TS (2011) An integrated passive micromixer–magnetic separation–capillary electrophoresis microdevice for rapid and multiplex pathogen detection at the single-cell level. *Lab Chip* 11:3465–3470
- Kim D, Oh H, Park T, Choo J, Lee SH (2005) An easily integrative and efficient micromixer and its application to the spectroscopic detection of glucose-catalyst reactions. *Analyst* 130:293–298
- Kitson PJ, Rosnes MH, Sans V, Dragone V, Cronin L (2012) Configurable 3D-Printed millifluidic and microfluidic ‘lab on a chip’ reactionware devices. *Lab Chip* 12:3267–3271. doi:10.1039/c2lc40761b
- Kong MC, Salin ED (2012) Micromixing by pneumatic agitation on continually rotating centrifugal microfluidic platforms. *Microfluid Nanofluid* 13:519–525
- Lai H, Folch A (2011) Design and dynamic characterization of “single-stroke” peristaltic PDMS micropumps. *Lab Chip* 11:336–342. doi:10.1039/c0lc00023j
- Lai H-C, Wang C-H, Liou T-M, Lee G-B (2014) Influenza A virus-specific aptamers screened by using an integrated microfluidic system. *Lab Chip* 14:2002–2013
- Lawton RA, Price CR, Runge AF, Doherty WJ, Saavedra SS (2005) Air plasma treatment of submicron thick PDMS polymer films: effect of oxidation time and storage conditions. *Colloids Surf, A* 253:213–215
- Lee JM, Zhang M, Yeong WY (2016) Characterization and evaluation of 3D printed microfluidic chip for cell processing. *Microfluid Nanofluid* 20:5
- Legge NR, Holden G, Schroeder H (1987) Thermoplastic elastomers: a comprehensive review. Carl Hanser Verlag, Munchen
- Ping Z, Nguyen Q, Chen S, Zhou J, Ding Y (2001) States of water in different hydrophilic polymers—DSC and FTIR studies. *Polymer* 42:8461–8467
- Plečis A, Chen Y (2007) Fabrication of microfluidic devices based on glass-PDMS-glass technology. *Microelectron Eng* 84:1265–1269. doi:10.1016/j.mee.2007.01.276
- Ratner DM, Murphy ER, Jhunjhunwala M, Snyder DA, Jensen KF, Seeberger PH (2005) Microreactor-based reaction optimization in organic chemistry glycosylation as a challenge. *Chem Commun*. doi:10.1039/b414503h
- Rose P, Mark H, Bikales N, Overberger C, Menges G, Kroschwitz J (1987) Encyclopedia of polymer science and engineering Mark, HF: 488
- Shankar R, Raravikar NR, Xu D (2010) Self-healing thermal interface materials for semiconductor packages
- Sochol R et al (2016) 3D printed microfluidic circuitry via multijet-based additive manufacturing. *Lab Chip* 16:668–678
- Spontak RJ, Patel NP (2000) Thermoplastic elastomers: fundamentals and applications. *Curr Opin Colloid Interface Sci* 5:334–341
- Stjernstrom M, Roeraade J (1998) Method for fabrication of microfluidic systems in glass. *J Micromech Microeng* 8:33–38. doi:10.1088/0960-1317/8/1/006
- Sundararajan N, Kim D, Berlin AA (2005) Microfluidic operations using deformable polymer membranes fabricated by single layer soft lithography. *Lab Chip* 5:350–354
- Thangawng AL, Ruoff RS, Swartz MA, Glucksberg MR (2007) An ultra-thin PDMS membrane as a bio/micro-nano interface: fabrication and characterization. *Biomed Microdevice* 9:587–595. doi:10.1007/s10544-007-9070-6
- Wang Z (2011) Polydimethylsiloxane mechanical properties measured by macroscopic compression and nanoindentation techniques. University of South Florida
- Wang JD, Douville NJ, Takayama S, ElSayed M (2012) Quantitative analysis of molecular absorption into PDMS microfluidic channels. *Ann Biomed Eng* 40:1862–1873
- Yao P, Tung S, Zhan Z, Hua J, Dong Z (2013a) Development of microfluidic-based telemedicine for diabetes care and screening. *Trans Inst Meas Control* 35:893–900. doi:10.1177/0142331212455449

- Yao P, Xie S, Liu Z, Dong Z, Liu L, Wang W, Tung S (2013) Combined experimental and numerical simulation study of PDMS pneumatic micropumps. In: Nano/Molecular medicine and engineering (NANOMED), 2013 IEEE 7th International Conference on, 2013b. IEEE, pp 130–133
- Yao P, Liu Z, Tung S, Dong Z, Liu L (2016) Fully automated quantification of insulin concentration using a microfluidic-based chemiluminescence immunoassay. *J Lab Autom* 21:387–393
- Young WC, Budynas RG (2002) Roark's formulas for stress and strain, vol 7. McGraw-Hill, New York
- Zhang WJ, Choi DS, Nguyen YH, Chang J, Qin LD (2013) studying cancer stem cell dynamics on PDMS surfaces for microfluidics device design. *Sci Rep* 3:8. doi:[10.1038/srep02332](https://doi.org/10.1038/srep02332)
- Zhou J, Ellis AV, Voelcker NH (2010) Recent developments in PDMS surface modification for microfluidic devices. *Electrophoresis* 31:2–16